The Journal of Nutrition
Biochemical, Molecular, and Genetic Mechanisms

Caco-2 Intestinal Epithelial Cells Absorb Soybean Ferritin by μ_2 (AP2)-Dependent Endocytosis[1,2]

Carol D. San Martin,[3] Carolina Garri,[3] Fernando Pizarro,[4] Tomas Walter,[4] Elizabeth C. Theil,[5,6] and Marco T. Núñez[3]*

[3]Department of Biology, Faculty of Sciences, and Cell Dynamics and Biotechnology Institute and [4]Nutrition and Food Technology Institute, Universidad de Chile, Santiago, Chile; [5]Council for BioIron at Children's Hospital Oakland Research Institute, Oakland, CA 94609; and [6]Department of Nutritional Sciences and Toxicology, University of California, Berkeley, CA 94720

Abstract

Iron deficiency, a condition currently affecting ~3 billion people, persists in the 21st century despite half a millennium of medical treatment. Soybean ferritin (SBFn), a large, stable protein nanocage around a mineral with hundreds of iron and oxygen atoms, is a source of nutritional iron with an unknown mechanism for intestinal absorption. Iron absorption from SBFn is insensitive to phytate, suggesting an absorption mechanism different from for the ferrous transport. Here, we investigated the mechanism of iron absorption from mineralized SBFn using Caco-2 cells (polarized in bicameral inserts) as an intestinal cell mode and analyzed binding, internalization and degradation with labeled SBFn (^{131}I or fluorescent labels), confocal microscopy, and immunoanalyses to show: *1*) saturable binding to the apical cell surface; dissociation constant of 7.75 ± 0.88 nmol/L; *2*) internalization of SBFn that was dependent on temperature, concentration, and time; *3*) entrance of SBFn iron into the labile iron pool (calcein quenching); *4*) degradation of the SBFn protein cage; and *5*) assembly peptide 2 (AP2)-/clathrin-dependent endocytosis (sensitivity of SBFn uptake to hyperosmolarity, acidity, and RNA interference to the μ_2 subunit of AP2), and resistance to filipin, a caveolar endocytosis inhibitor. The results support a model of SBFn endocytosis through the apical cell membrane, followed by protein cage degradation, mineral reduction/dissolution, and iron entry to the cytosolic iron pool. The large number of iron atoms in SBFn makes iron transport across the cell membrane a much more efficient event for SBFn than for single iron atoms as heme or ferrous ions. J. Nutr. 138: 659–666, 2008.

Introduction

Cells transport nutrient iron from foods by mechanisms related to the type of iron complex, such as endocytosis for Fe-transferrin from blood and, in the gut, membrane transporters such as heme carrier protein 1 (HCP1)[7] for heme (myoglobin) (1) and divalent metal transporter 1 (DMT1) for ferrous and other divalent cations (2–5). Current data indicate that after internalization, iron from heme or inorganic sources becomes part of the cytosolic labile iron pool (LIP) [reviewed in (6)] and is either concentrated and stored in ferritin or moved to the basolateral membrane for efflux; this latter process is dependent on the iron-export transporter ferroportin, also known as Iron Regulated Gene 1 (7–9), in combination with the ferrous oxidase hephaestin (10).

Recent studies show that ferritin iron, a biomineral inside a large stable protein nanocage, can be absorbed from foods such as legumes, a particularly rich source [reviewed in (11,12)]. The cellular mechanism used to absorb ferritin iron is unknown, but because ferritin is a very stable protein (13,14) and ferritin iron can be absorbed from soybean ferritin (SBFn) even in the presence of iron-binding inhibitors such as phytate (15), it is possible that the mechanism differs from that used to transport lower molecular weight iron complexes. High-affinity mammalian ferritin binding sites have been reported in reticulocytes, lipocytes, hepatocytes, placenta, brain, and kidney (16–19), although the mechanism of ferritin endocytosis has not been elucidated. We investigated possible mechanisms of ferritin uptake using fluorescence microscopy, calcein quenching, and ^{131}I-SBFn binding, uptake, and degradation assays in the intestinal epithelial cell line, Caco-2, as a model for polarized epithelial cells.

Materials and Methods

Ferritin protein

SBFn was isolated from the clarified supernatant fractions as we previously described (20) using chromatography on DEAE-Sephadex and Sephacryl S300. SBFn purity was evaluated by electrophoresis in both SDS and native gels, calibrated with molecular weight markers, and

[1] Supported by grant 1050068 from the Fondo Nacional de Desarrollo Científico y Técnológico, Chile (to C.G., F.P., C.S.M., M.T.N., and T.W.) and by NIH grant DK20251 (to E.C.T.).
[2] Author disclosures: C. D. San Martin, C. Garri, F. Pizarro, T. Walter, E. C. Theil, and M. T. Núñez, no conflicts of interest.
[7] Abbreviations used: AP2, assembly peptide 2; DMT1, divalent metal transporter 1; FAS, ferrous ammonium sulfate; HCP1, heme carrier protein 1; HSFn, horse spleen ferritin; K_D, dissociation constant; LIP, labile iron pool; SBFn, soybean ferritin; TCA, trichloroacetic acid.
* To whom correspondence should be addressed. E-mail: mnunez@uchile.cl.

Manuscript received 7 September 2007. Initial review completed 6 November 2007. Revision accepted 17 January 2008.

stained with Coomassie Blue. Purity was >90%. The isolated protein also reacted with SBFn antiserum followed by incubation with horseradish peroxidase-conjugated anti-rabbit IgG and a peroxidase-based chemiluminescence assay kit (ECL+, Bio-Rad).The iron content of a typical preparation was 450 Fe per protein nanocage. Purified protein was stored at 4°C in 0.2 mol/L MOPS, 0.2 mol/L NaCl, pH 7.0, or frozen at –20°C in 20% glycerol.

^{131}I-labeling of SBFn

SBFn was labeled with ^{131}I (5 mCi/mg protein) using the Iodogen reagent (Pierce Chemical). After iodination, ^{131}I-labeled SBFn was separated from free ^{131}I by 50% ammonium sulfate precipitation followed by extensive dialysis against saline containing the anionic resin AG1 ×8 (Bio-Rad) to eliminate adventitiously bound ^{131}I. ^{131}I-labeled SBFn was stored at 4°C and used within 10 d after labeling.

Binding of ^{131}I-labeled SBFn and horse spleen ferritin to Ca*co-2* cells

Human Caco-2 cells (ATCC HTB37) grown on plastic wells for 12–14 d in DMEM supplemented with 10% fetal bovine serum were incubated in serum-free DMEM with concentrations of ^{131}I-labeled SBFn or horse spleen ferritin (HSFn) that varied between 1 and 40 nmol/L, with or without the addition of 100-fold excess unlabeled ferritin. Binding was performed for 2 h at 4°C. Cells were washed 5 times with ice-cold PBS and detached from the plates with 200 μL 40 mmol/L Tris-HCl, pH 7.4, 100 mmol/L NaCl, 1 mmol/L EDTA for 10 min and then collected by centrifugation at 390 × *g*; 5 min (Hettich Mikro 22R centrifuge). Cell-associated ^{131}I radioactivity was determined in a Cobra II Gamma Radioactivity Counting System (Packard). An aliquot of the cell suspension was used for protein determination with bicinchoninic acid (21). Each data point was determined in triplicate. Specific binding was calculated by subtracting binding of ^{131}I-labeled SBFn or HSFn in the presence of an excess of the corresponding unlabeled ferritin, from binding in the absence of excess, unlabeled SBFn. Binding data were analyzed using GraphPad Prism software (GraphPad Software).

^{131}I-SBFn internalization and degradation

Internalization of ^{131}I-SBFn protein was determined by incubating Caco-2 cells in DMEM with 5 nmol/L ^{131}I-SBFn for 0, 15, 30, 60, 90, and 120 min at 37°C. The cells were washed 5 times with ice-cold PBS, detached from the plastic with 200 μL of 40 mmol/L Tris-HCl, pH 7.4, 100 mmol/L NaCl, 1 mmol/L EDTA, and collected by centrifugation. The cells were resuspended in 200 μL PBS and incubated overnight at 4°C with 500 nmol/L unlabeled SBFn. Cells were then centrifuged and the supernatant and pellet fractions were analyzed for ^{131}I radioactivity as described above. Radioactivity in the supernatant represented surface-bound SBFn and radioactivity in the cell pellet represented internalized SBFn. To measure ^{131}I-SBFn degradation products, the incubation medium was precipitated for 30 min on ice with 10% trichloroacetic acid (TCA). Then 10 μL of FBS was added as carrier protein to obtain a visible pellet. The mixture was separated into precipitate and supernatant fractions by centrifugation at 9860 × *g*; 5 min in a Mikro 22R centrifuge. Radioactivity in the supernatant and precipitated fractions of the culture medium represented degraded and nondegraded ^{131}I-SBFn, respectively (22–24).

Inhibition of SBFn endocytosis

Caco-2 cells grown in Transwell inserts were incubated for 60 min at 37°C with 5 nmol/L ^{131}I-SBFn in the following media: DMEM (control); DMEM plus 5 mg/L Filipin III (Sigma); DMEM plus 0.45 mol/L sucrose (hypertonic), and DMEM with 10 mmol/L acetic acid (cytosol acidification). The cells were washed and surface-bound ferritin was displaced by an overnight incubation at 4°C with 500 nmol/L SBFn. The remaining cell-associated ^{131}I radioactivity represented intact, internalized SBFn.

Confocal microscopy

Fluorescent reporter linked to secondary antibody. SBFn (5 nmol/L) was added to polarized Caco-2 cells grown on glass cover slips followed by incubation for 60 min. Cells were then fixed and permeabilized, blocked, and incubated overnight with anti-SBFn rabbit antiserum diluted 1:100 (20), washed, incubated 1 h with Alexa 488-labeled anti-rabbit IgG (Invitrogen-Molecular Probes), and viewed with a Zeiss LSM510 Meta confocal microscope (Carl Zeiss AG).

Fluorescent reporter linked to ferritin. SBFn was coupled to Oregon Green 488 using the FluoReporter Oregon Green 488 Protein Labeling kit (Invitrogen-Molecular Probes) to yield SBFn-OG488. Polarized Caco-2 cells cultured on cover slips for 12–14 d were incubated for 60 min at 37°C with 5 nmol/L SBFn-OG488 in the absence or presence of 500 nmol/L unlabeled SBFn. After washing, the cells were fixed with 4% paraformaldehyde, mounted in Gel Mount (Sigma), and observed with a Zeiss LSM 510 Meta confocal laser scanning microscope. By this method, Oregon Green fluorescence reported both intact SBFn and its degradation products.

Transfections

Lipofectamine. Polarized Caco-2 cells were transfected with DNA encoding a short hairpin RNA directed against the μ_2 (AP50) subunit of the assembly peptide 2 (AP2) endocytic complex (25). The plasmid pSUPER, encoding the μ_2 target sequence GTGGATGCCTTTCGGGTCA (25), was the kind gift of Dr. Philippe Benaroch, INSERM U520 Institut Curie, Paris, France. Caco-2 cells grown for 10 d (60% confluence; 8×10^5 cells) were treated with 2.5 μg DNA in lipofectamine (Gibco) for 36 h at 37°C as previously described (26); transfection efficiencies were 20–25%. Lipofectamine-transfected cells were used for immunocytochemistry of μ_2.

Electroporation. Caco-2 cells grown as above were nucleofected with pSUPER containing the μ2 target sequence using a Nucleofector device and the Caco-2 transfection kit following the manufacturer's protocol (amaxa GmbH). Nucleofected cells, 3–4 d after transfection when the transfection efficiency was ~65–75%, were analyzed for SBFn internalization and μ_2 protein expression (Western blot).

Western blot analysis of μ_2

Cell extracts from control and μ_2-electroporated cells were prepared by treating cells with lysis buffer [50 μL/1 × 10^6 cells of 10 mmol/L MOPS, pH 7.5, 3 mmol/L $MgCl_2$, 40 mmol/L KCl, 1 mmol/L phenylmethylsulfonyl fluoride, 10 mg/L leupeptin, 0.5 mg/L aprotinin, 0.7 mg/L pepstatin A, 5% glycerol, 1 mmol/L dithiothreitol, 0.1% Triton X-100]. The mixture was incubated for 15 min on ice and then fractionated by centrifugation at 5000 × *g*; 10 min. Protein concentrations were determined using the bicinchoninic acid protein assay. The supernatant fraction was stored at −70°C (27). For Western blotting, samples containing 100 μg of protein were boiled in Laemmli sample buffer for 5 min and the denatured proteins resolved by SDS-PAGE (10% acrylamide). Proteins were transferred to nitrocellulose membrane and blocked for 1 h at 25°C with 5% nonfat dry milk in blocking saline [20 mmol/L Tris, 0.5 mol/L NaCl, 0.05% (wt:v) Tween-20]. Membranes were incubated overnight at 4°C with anti-μ_2 at a 1:200 dilution, rinsed with blocking saline, and incubated with horseradish peroxidase-conjugated anti-mouse IgG for 1 h at 25°C. A chemiluminescence assay kit was used for detection (SuperSignal, Pierce Chemical). Chemiluminescence was detected with Fuji photographic film and the band density was determined with the Quantity One (Bio-Rad) program.

Determination of iron incorporation with calcein

Polarized Caco-2 cells grown in 2-cm tissue culture wells were incubated for 15 min at 37°C in Hanks' Balanced salt solution containing 5 mmol/L glucose and 1 μmol/L calcein as the lipophilic, acetoxymethyl ester calcein-AM (Invitrogen-Molecular Probes). Calcein-AM is hydrolyzed by intracellular esterases to the membrane-impermeable calcein. The decreased calcein fluorescence (485 nm excitation, 530 nm emission) after adding SBFn or ferrous ammonium sulfate (FAS) was quantified using a Cytofluor II plate reader (Applied Biosystems). After stabilization of the background calcein fluorescence in cells, the medium was supplemented with either 10 nmol/L SBFn or 10 μmol/L FAS and changes in calcein fluorescence were monitored for the next 20 min. Calcein photobleaching was measured in control cells incubated in parallel. Typically, at the end of 20 min, calcein photobleaching was <2% of the initial calcein fluorescence. To eliminate possible interference from nonmineral iron, SBFn was treated with 10

mmol/L diethylenetriaminepentaacetic acid and dialyzed against DMEM prior to the experiment.

Statistical analysis

The data presented are triplicate analyses from 2 or more independent experiments. Experimental variability was <20%. One-way ANOVA was used to test for significant differences among mean values and Tukey's post hoc test was used for comparisons (InStat, GraphPad Software). Differences were considered significant if $P < 0.05$.

Results

SBFn protein binding, internalization, and degradation by Caco-2 cells. Apical internalization of SBFn was demonstrated by immunofluorescence using an antibody specific for SBFn (**Fig. 1**); SBFn polypeptides >10 kDa are immunoreactive (22). Overlays of fluorescence and phase contrast images from cells, incubated without or with SBFn prior to immunodetection, showed the specificity of anti-SBFn (Fig. 1*A*). There was a gradient of decreasing immunoreactivity as the distance from the apical surface of the cell increased, with most of the reactivity in the apical half of the cells (Fig. 1*B*,*C*).

Specific binding of SBFn to the apical surface of Caco-2 cells. To determine the properties of SBFn interactions with the apical membrane of Caco-2 cells, we analyzed binding of SBFn labeled with ^{131}I to the apical membrane Caco-2 cells (**Fig. 2**). Binding of ^{131}I-labeled HSFn was also determined. Nonspecific binding, determined as the ^{131}I radioactivity remaining after incubation in the presence of unlabeled SBFn (100-fold excess), was subtracted from total ^{131}I radioactivity. Nonspecific binding

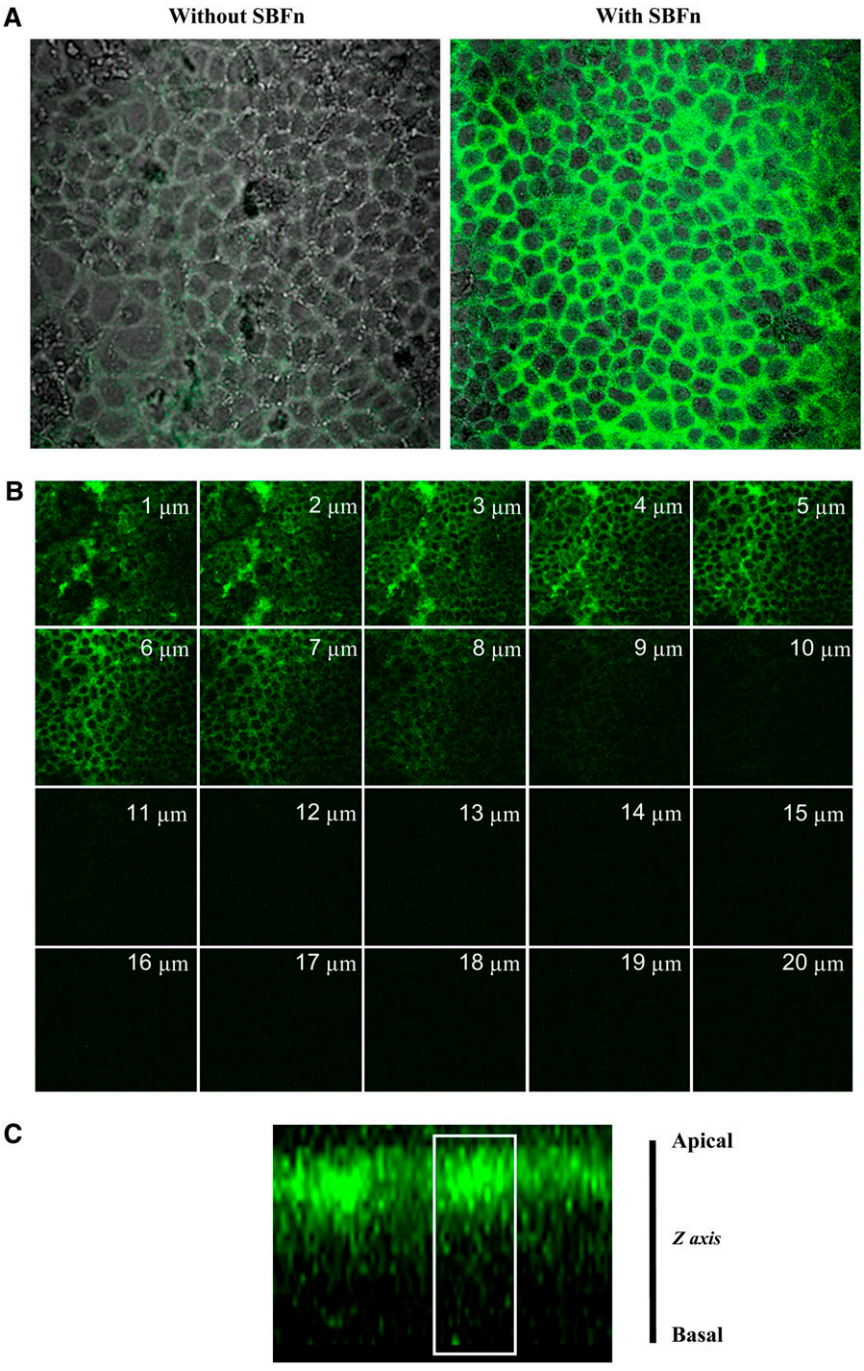

FIGURE 1 Immunofluorescence detection of SBFn inside cells. (*A*) Caco-2 cells grown on glass cover slips were incubated for 60 min with 5 nmol/L SBFn. Cells were then fixed and permeabilized, incubated with anti-SBFn rabbit antiserum, detected with Alexa 488-labeled anti-rabbit IgG, and viewed under a confocal microscope. Overlays of fluorescence and phase contrast images from cells incubated without or with SBFn prior to immunodetection, showing that the antibody did not label endogenous Caco-2 cell ferritin. (*B*) Gallery of 1-μm optical slices from the apical to basal membrane. Staining for SBFn was prominent in the apical domain. (*C*) Z-axis projection of confocal optical slices revealing SBFn immunoreactivity mostly in the upper half of the cell. A cell contour, in white, derived from phase contrast images, is shown as a reference.

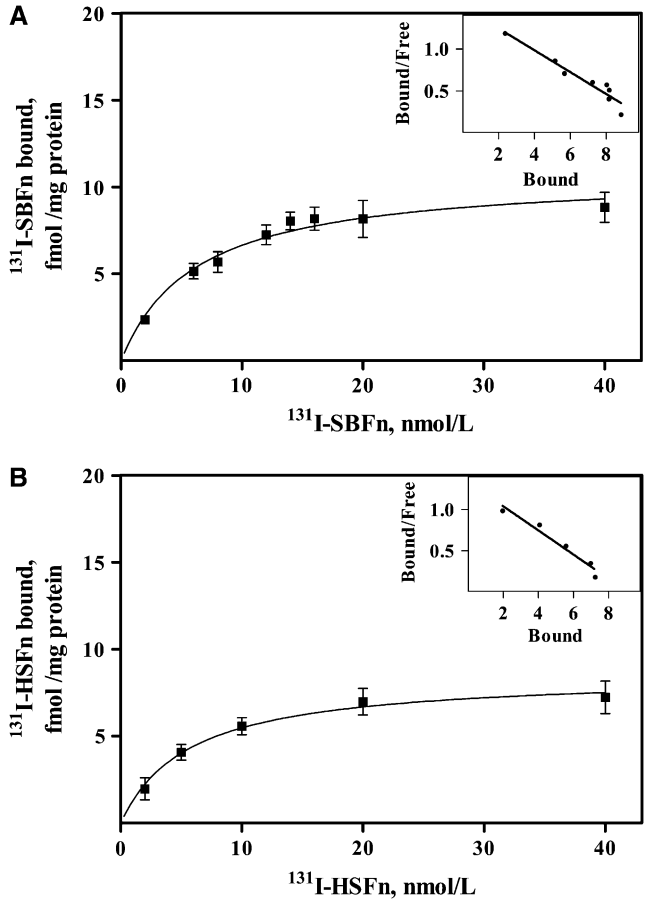

FIGURE 2 Binding of ^{131}I-labeled SBFn and HSFn. (*A,B*) Caco-2 cells grown in bicameral transwells were incubated from the apical chamber for 2 h at 4°C with various concentrations of either ^{131}I-labeled SBFn (*A*) or HSFn (B). The data are the differences in ^{131}I between cells incubated with or without unlabeled (100-fold molar excess) SBFn (*A*) or HSFn (*B*). Data points were fit with the hyperbolic function in GraphPad 5.0. The results are the means of 4 (SBFn) or 3 (HSFn) independent experiments and the error is SEM. Inserts, Scatchard analysis of binding data.

was ~15% of specific binding at 10 nmol/L ^{131}I-SBFn. The binding data were adjusted with the hyperbolic function in GraphPad 5.0. Scatchard analysis indicated an apparent K_D of $7.75 \pm 0.84 \times 10^{-9}$ mol/L for SBFn (Fig. 2*A*) and $6.82 \pm 0.89 \times 10^{-9}$ mol/L for HSFn (Fig. 2*B*). These values are similar to K_D values of 5.1×10^{-10} mol/L, 4.1×10^{-8} mol/L, and 4.65×10^{-9} mol/L for ferritin binding to lipocytes (18), erythroid precursors (28), and mouse brain (19), respectively. These results suggest the presence of specific receptors in the apical surface of Caco-2 cells that recognize ferritin of both plant and animal origin.

Fate of internalized SBFn protein. The kinetics of binding of SBFn by Caco-2 cells was investigated by incubating Caco-2 cells with ^{131}I-labeled SBFn in the apical medium (**Fig. 3***A*). The rate of binding in the initial phase was 0.73 ± 0.13 fmol/mg protein. Steady-state binding was attained in ~30 min of incubation. After 1 h incubation at 37°C, ^{131}I-SBFn surface binding was 1.5 ± 0.4 fmol/mg cell protein. Based on the percent TCA insoluble I^{131}-protein, we conclude that the majority of the cell-associated ^{131}I-SBFn (87.3 ± 4.4%) was intact protein. This ^{131}I-SBFn was inside the cells, because it was not displaced from the cell in an overnight incubation at 4°C with 500 nmol/L unlabeled SBFn. The amount of ^{131}I in the medium after 1 h of incubation was equivalent to 130.3 ± 15.6 fmol/mg protein compared with 10.0 ± 1.4 fmol/mg protein of intact ^{131}I-SBFn inside the cells (Fig. 3*B*). These values indicate that SBFn was degraded quickly after internalization and the degradation products were released into the medium. Moreover, actively metabolizing cells were necessary to convert the internalized ^{131}I-SBFn to TCA-soluble ^{131}I in the medium, because incubation with or without cells at 4°C, or without cells at 37°C, converted only ~5% of the ^{131}I-SBFn to TCA-soluble fragments (Fig. 3*C*).

Fate of the iron in internalized SBFn. A measure of the biological availability of absorbed ferritin iron is entry into the

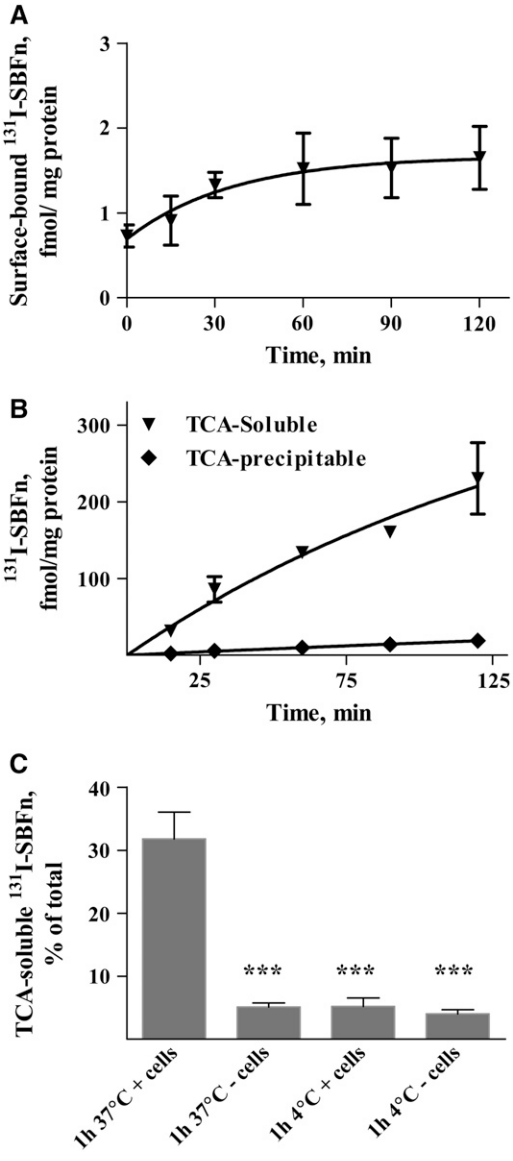

FIGURE 3 Fate of SBFn in Caco-2 Cells. (*A*) Polarized Caco-2 cells were incubated with 5 nmol/L ^{131}I-labeled SBFn at 37°C for different times. Protein binding to the cell surface, determined by displacement of surface ^{131}I-labeled SBFn by unlabeled SBFn. (*B*) Protein degradation, determined as the soluble ^{131}I radioactivity following 10% TCA precipitation, was measured as described previously. (*C*) The effects of cells and temperature on the release of ^{131}I-ferritin degradation products were analyzed as described previously. Values are means ± SEM, $n = 3$ independent experiments (means of triplicates). ***Different from controls (1 h, 37°C, + cells), $P < 0.001$.

LIP, which corresponds to iron bound with low affinity to a variety of cytosolic ligands (29). To determine whether ferritin iron becomes available to the cell cytoplasm when the mineralized protein is internalized by Caco-2 cells, we measured calcein fluorescence, which is quenched upon binding either Fe^{+2} or Fe^{+3} (30,31). Calcein fluorescence decreased with time when either mineralized HSFn or mineralized SBFn was used as the iron source, indicating that iron from either source entered the cytosolic LIP (**Fig. 4***A*). Desferal did not inhibit iron incorporation from HSFn, an indication that HSFn did not have adventitious iron. FAS iron, which enters cells via the DMT1 transporter, was used as a positive control (32) and the fluorescence of cell calcein without added iron was followed to assess calcein photobleaching during the experiment. As a negative control, the iron-donating capacity of apoSBFn was determined. No changes in calcein fluorescence were observed with apoSBFn (data not shown). Changes in calcein fluorescence were best fit to a 1-phase, exponential decay model. The steady state in calcein quenching probably reflects a balance between iron influx into the cytosol and iron traffic to other subcellular compartments.

Because previous studies have detected surface ferritin receptors (16–19) and because the size of ferritin would require endocytosis as a cellular internalization process, we tested the effects of interfering with clathrin-coated pit function on the entry of ferritin iron into the LIP. Interference with normal clathrin-coated vesicles was achieved by cytoplasmic acidification, which interferes with budding of clathrin-coated vesicles from the plasma membrane and by incubation in hypertonic medium, which prevents clathrin and AP2 from interacting (33–35) (Fig. 4*B*).

The effect of SBFn concentration on the LIP was also determined (Fig. 4*C*,*D*). Increased SBFn concentration resulted in increased initial rates of calcein quenching, which reached a plateau (Fig. 4*C*). Plotting the initial rate of iron entrance as a function of SBFn concentration resulted in a hyperbolic curve with an apparent K_D of $4.53 \pm 0.61 \times 10^{-9}$ mol/L, a value close to the K_D of ^{131}I-SBFn ($7.75 \pm 0.84 \times 10^{-9}$ mol/L) (Fig. 4*D*), a clear indication that most of the mineralized iron from SBFn or HSFn that was specifically bound to the cell was available to the LIP.

Inhibition of SBFn internalization by acidification and hyperosmolarity and insensitivity of internalization to filipin. To further investigate the pathway(s) of SBFn protein internalization in human intestinal epithelial Caco-2 cells, we examined the subcellular distribution of SBFn labeled with Oregon Green after incubation for different periods of time (**Fig. 5***A*). After a 5-min incubation with Oregon-green-ferritin, most of the label was at the apical membrane, as it was for the fluorescent immunoanalysis (Fig. 1). However, after longer periods of incubation, an apical-to-basal gradient of the label was observed (Fig. 5), with intracellular fluorescence increasing up to 30 min, when signals in the apical, cytosolic, and basal domains were evident, a contrast with the immunofluorescent analysis (Fig. 1). The signal from Oregon green-labeled SBFn on the basal side of the cell likely indicates degraded SBFn fragments that remain linked to Oregon Green and suggests that internalized SBFn is degraded in an apical-to-basal direction.

Effects of inhibitors of caveolar- or clathrin-dependent endocytosis of Oregon green-SBFn ferritin were studied by preincubating cells with inhibitors and analyzing the effect either on the distribution of Oregon Green-labeled SBFn (Fig. 5 *A*,*B*) or on uptake of ^{131}I-labeled SBFn (Fig. 5*C*). Inhibitors of clathrin-mediated endocytosis (hypertonicity or cytosol acidification) changed the distribution of Oregon Green fluorescence, which was concentrated at the apical limit contrasting with control cells fluorescence (Fig. 5*B*). Filipin, a sterol-binding agent that disrupts cholesterol microdomains in caveolae but does not influence clathrin-dependent endocytosis (36–38), did not affect SBFn internalization (Fig. 5*B*); the slight decrease in retention of the labeling in the apical membrane of filipin-treated cells likely reflects the impact of Filipin on the membrane structure. Inhibitors of clathrin-dependent endocytosis had similar effects on ^{131}I-labeled SBFn internalization, which was also resistant to

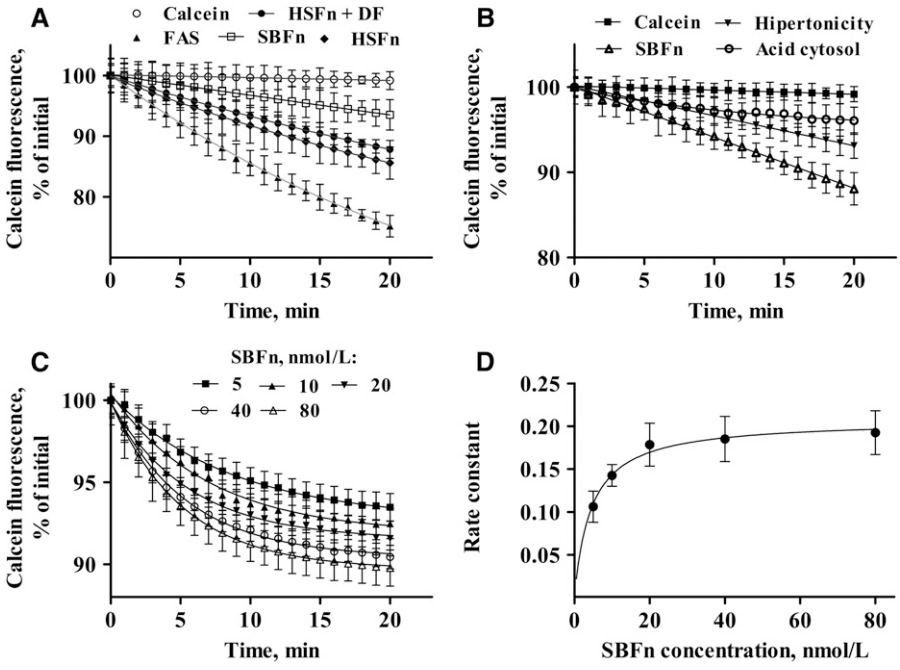

FIGURE 4 Incorporation of SBFn iron into the LIP. Entry of exogenous iron into polarized calcein-loaded Caco-2 cells was measured as the quenching of calcein fluorescence. Fluorescence was monitored every minute for 20 min; calcein photobleaching during the experiment, determined in parallel using cells without added iron, was <2%. (*A*) Ferritin and iron salts: 10 μmol/L FAS, 10 nmol/L HSFn, 10 nmol/L HSFn + 10 μmol/L desferal, and 10 nmol/L SBFn. (*B*) Ferritin, iron salts, and inhibitors of endocytosis: 10 nmol/L SBFn in DMEM (SBFn), DMEM + 10 mmol/L acetic acid pH 5.0 (acid), or DMEM + 0.45 mol/L sucrose (hyper). (*C*) SBFn protein concentrations ranging from 5–80 nmol/L. (*D*) Rate constants derived from Figure 5*C* plotted as a function of SBFn concentration. The data were fit to a single exponential decay function using the GraphPad 5.0 program. Values in panels *A*–*C* are means ± SEM, $n = 3$ representative experiments (means of triplicates). Values in panel *D* are means ± SEM, $n = 3$ experiments.

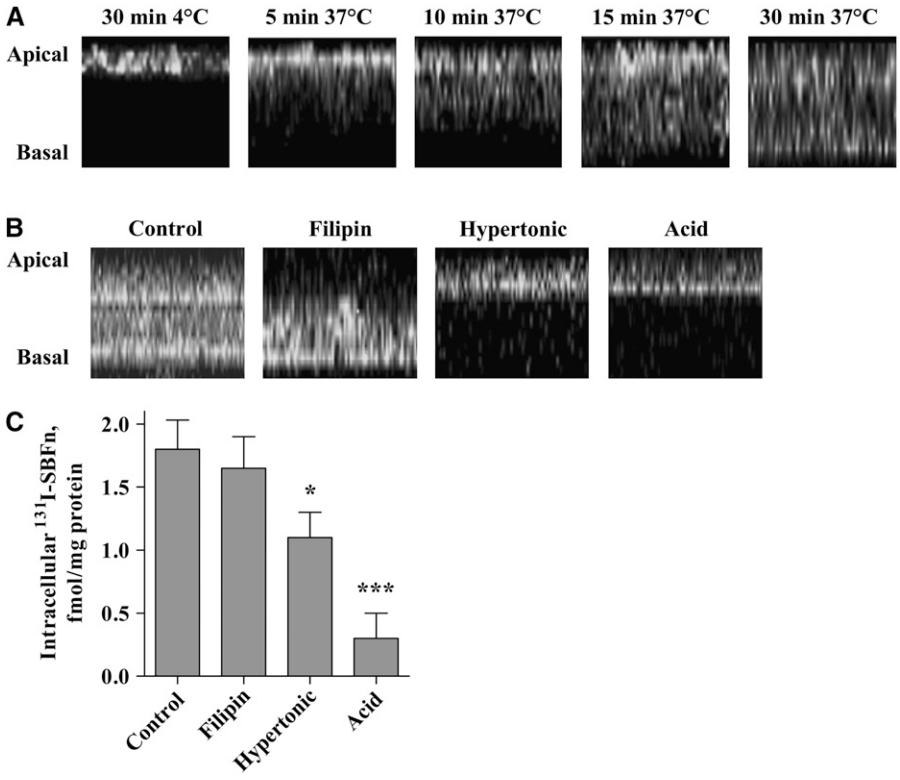

FIGURE 5 Effects of endocytic inhibitors on SBFn endocytosis. (*A*) Polarized Caco-2 cells, grown in transwell inserts, were incubated for 0–30 min at 37°C with 5 nmol/L SBFn labeled with Oregon Green 488 and a gallery of confocal fluorescence microscopy optical slices were obtained and integrated into a Z-axis projection; with longer incubation, the initial concentration of fluorescence at the apical domain decayed to fluorescence throughout the cytosol, likely due to Oregon Green-labeled, protein degradation products. (*B*) Cells were incubated with Oregon Green-labeled SBFn (10 μmol/L) for 60 min at 37°C after preincubation (15 min) with or without the inhibitors of endocytosis filipin, or hypertonicity or acetic acid as described previously. (*C*) Cells were incubated with ^{131}I-labeled SBFn (5 nmol/L) for 60 min at 37°C after preincubation (15 min) with or without the inhibitors of endocytosis filipin, or hypertonicity or acetic acid. Values are means ± SEM, $n = 3$ independent experiments. *Different from control, $P < 0.05$; ***$P < 0.001$.

filipin (Fig. 5*C*). The inhibitor data (Fig. 5), combined with those from the calcein study (Fig. 4), indicate that both Fe transfer from SBFn to the LIP and SBFn protein internalization depend on an AP2-mediated pathway.

Inhibition of SBFn internalization by RNA interference of μ_2, a subunit of the AP2 complex. More direct data for the dependence of SBFn uptake on AP2 was sought with RNA interference for the μ_2 subunit of the AP2 endocytic complex (**Fig. 6**). Western blot analysis of transfected cells revealed decreased expression of the μ_2 protein (Fig. 6*A*), which correlated with decreased intracellular SBFn, i.e. decreased ^{131}I-labeled SBFn uptake (Fig. 6*B*). IgG uptake by intestinal cells, which depends on by clathrin-mediated endocytosis (39,40), was also inhibited by μ_2 RNA interference (Fig. 6*B*). The sensitivity of ferritin and IgG internalization to μ_2 expression supports the hypothesis that ferritin uptake is facilitated by an AP2-mediated endocytosis pathway.

Discussion

Recent studies show that ferritin iron is absorbed by mammals from plant ferritin [reviewed in (12)]. This observation is potentially important for the treatment of iron deficiency anemia, a condition affecting ~3 billion people in the 21st century despite half a millennium of medical diagnoses and treatments. Moreover, the difference in the structure of ferritin iron, a solid mineral of hundreds to thousands of atoms inside a large, hydrophilic protein cage, compared with the single iron atoms in lipid-soluble heme or the single ferrous ion coordinated to 6 water molecules raises the possibility that ferritin is recognized by different molecules on the surface of intestinal cells compared with the more extensively studied forms of iron in heme and ferrous salts. All cells synthesize ferritin, the spherical, protein nanocages with iron biominerals inside, at some time during differentiation or maturation (41). In animal cells, in addition to the generic Fer H-type gene found universally in animals, plants and bacteria, a catalytically inactive subunit, FerL, is expressed that coassembles with the FerH subunit in variable amounts (42,43), making endogenous intestinal cell ferritin different from plant ferritin. Each plant ferritin subunit also has a distinctive N-terminal extension (20).

In this study, we showed that SBFn entered cells from the apical surface of Caco-2 cells by an AP2-mediated endocytic pathway. Based on the calcein fluorescence quenching data, once internalized, SBFn iron entered the common intracellular iron pool, indicating the physiological relevance of ferritin uptake, and the SBFn protein was degraded, as demonstrated by the release of ^{131}I into the TCA-soluble fraction of the medium. Because steady-state SBFn binding occurs later (~30 min) than calcein quenching (1–2 min) (Figs. 3,4), the data do not distinguish among iron release before protein degradation from intact molecules (43) or after protein degradation (12) or both. Thus, gut absorption of plant ferritin via ferritin endocytosis could provide iron for bodily needs and may explain the presence of ferritin-rich legumes among the earliest plants domesticated by humans (44).

Endocytosis of iron as the ferritin mineral is much more efficient transport event than transport of individual iron atoms across the cell membrane as ferrous iron via DMT1 or heme via HCP1, e.g., as the ferritin mineral usually contains hundreds to thousands of iron atoms (42,43). As found in nature, the SBFn used in this study was only partly filled with mineral (20) and contained an average of 450 ferric atoms. Therefore, in only 1 endocytosis event, a SBFn molecule releases to the cytosol an amount of iron equivalent to 450 iron-transport events through DMT1. The contribution of the 450 Fe atoms from ferritin internalized at the observed rate of 130 fmol degraded ferritin·h^{-1}·mg protein^{-1} would be 58 pmol Fe·h^{-1}·mg protein^{-1}, a value comparable to uptake values of 30 and 108 pmol Fe·h^{-1}·mg protein^{-1} for nonheme and heme iron by Caco-2 cells, respectively (45,46).

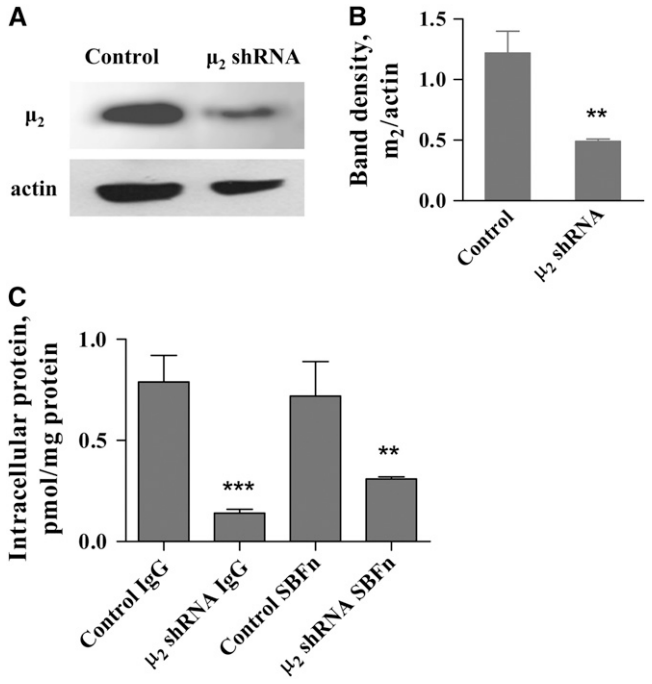

FIGURE 6 Inhibition of SBFn endocytosis by μ_2 RNA interference. (*A*) Cells were nucleofected with pSUPER or pSUPER-μ_2- short hairpin RNA plasmids and 3 d later tested for μ_2 expression by Western blot analysis. (*B*) Densitometric analysis of the data in A. (*C*) Cells nucleofected and analyzed after 3 d for internalization of ^{131}I-SBFn (10 nmol/L) or ^{131}I-IgG (15 nmol/L) after incubation for 60 min at 37°C. Values in *A* are means ± SEM, $n = 3$ independent experiments and in *C* from 1 representative experiment, (means of triplicates). (*B*) **Different from control, $P = 0.002$. (C) **Different from control, $P < 0.01$; ***$P < 0.001$.

Ferritin uptake has been observed in liver hepatocytes (47), lipocytes (18), erythroid precursors (28), mouse brain (19), and placental microvilli membrane (16). The finding that Ig-domain and mucin-domain protein 1 in kidney and liver is a specific receptor for endogenous H-ferritin in mouse (17) complemented earlier studies of saturable cell surface sites as participants in ferritin uptake. In addition, the suggestion of gut iron resorption from endogenous ferritin released during enterocyte turnover (48) could depend on ferritin/cell surface interactions. Regulation of ferritin uptake by cellular iron status has been observed for some cell types, such as erythroid precursors and cells in the placental microvilli (16,28), but iron regulation is absent in liver hepatocytes (47), possibly because of the specialized role of hepatocytes in storing excess body iron. Ferritin uptake by endocytosis through the apical membrane of Caco-2 cells is an extremely efficient uptake of iron through the cascade of ferritin internalization, mineral dissolution, and iron release.

Current molecular knowledge of cellular iron transport is limited to entry of ferrous ions (DMT1) or heme (HCP1) on the apical surface and the release of ferrous via ferroportin at the basolateral surface of gut absorptive epithelial cells. How iron moves from one side of the cell to the other, and where, and/or whether the 2 pathways converge within the cell have remained a mystery. SBFn endocytosis, identified here in intestinal Caco-2 cells, easily distinguished immunologically from endogenous ferritin, may be a valuable tool for tracking iron across cells, identifying the point(s) of convergence in trafficking of the different iron complexes entering cells by different pathways, and for a more complete understanding of iron nutrition from different sources.

Acknowledgments

The authors are grateful to Brie Fuqua for the isolation of SBFn and to Victoria Tapia and Lorena Sarragoni for help with confocal microscopy.

Literature Cited

1. Shayeghi M, Latunde-Dada GO, Oakhill JS, Takeuchi K, Laftah AH, Halliday N, Khan Y, Warley A, McCann FE, et al. Identification of an intestinal heme transporter. Cell. 2005;122:789–801.
2. Fleming MD, Romano MA, Su MA, Garrick LM, Garrick MD, Andrews NC. Nramp2 is mutated in the anemic Belgrade (b) rat: evidence of a role for Nramp2 in endosomal iron transport. Proc Natl Acad Sci USA. 1998;95:1148–53.
3. Fleming MD, Trenor CC III, Su MA, Foernzler D, Beier DR, Dietrich WF, Andrews NC. Microcytic anaemia mice have a mutation in Nramp2, a candidate iron transporter gene. Nat Genet. 1997;16:383–6.
4. Garrick MD, Dolan KG, Horbinski C, Ghio AJ, Higgins D, Porubcin M, Moore EG, Hainsworth LN, Umbreit JN, et al. DMT1: a mammalian transporter for multiple metals. Biometals. 2003;16:41–54.
5. Gunshin H, Mackenzie B, Berger UV, Gunshin Y, Romero MF, Boron WF, Nussberger S, Gollan JL, Hediger MA. Cloning and characterization of a mammalian proton-coupled metal-ion transporter. Nature. 1997;388:482–8.
6. Kruszewski M. Labile iron pool: the main determinant of cellular response to oxidative stress. Mutat Res. 2003;531:81–92.
7. Donovan A, Brownlie A, Zhou Y, Shepard J, Pratt SJ, Moynihan J, Paw BH, Drejer A, Barut B, et al. Positional cloning of zebrafish ferroportin1 identifies a conserved vertebrate iron exporter. Nature. 2000;403:776–81.
8. McKie AT, Marciani P, Rolfs A, Brennan K, Wehr K, Barrow D, Miret S, Bomford A, Peters TJ, et al. A novel duodenal iron-regulated transporter, IREG1, implicated in the basolateral transfer of iron to the circulation. Mol Cell. 2000;5:299–309.
9. Abboud S, Haile DJ. A novel mammalian iron-regulated protein involved in intracellular iron metabolism. J Biol Chem. 2000;275:19906–12.
10. Frazer DM, Vulpe C, McKie AT, Wilkins SJ, Trinder D, Cleghorn GJ, Anderson GJ. Cloning and gastrointestinal expression of rat hephaestin: relationship to other iron transport proteins. Am J Physiol Gastrointest Liver Physiol. 2001;281:G931–9.
11. Briat JF, Lobreaux S, Grignon N, Vansuyt G. Regulation of plant ferritin synthesis: how and why. Cell Mol Life Sci. 1999;56:155–66.
12. Theil EC. Iron, ferritin, and nutrition. Annu Rev Nutr. 2004;24:327–43.
13. Listowsky I, Blauer G, Enlard S, Betheil JJ. Denaturation of horse spleen ferritin in aqueous guanidinium chloride solutions. Biochemistry. 1972;11:2176–82.
14. Santambrogio P, Levi S, Arosio P, Palagi L, Vecchio G, Lawson DM, Yewdall SJ, Artymiuk PJ, Harrison PM, et al. Evidence that a salt bridge in the light chain contributes to the physical stability difference between heavy and light human ferritins. J Biol Chem. 1992;267:14077–83.
15. Murray-Kolb LE, Welch R, Theil EC, Beard JL. Women with low iron stores absorb iron from soybeans. Am J Clin Nutr. 2003;77:180–4.
16. Liao QK, Kong PA, Gao J, Li FY, Qian ZM. Expression of ferritin receptor in placental microvilli membrane in pregnant women with different iron status at mid-term gestation. Eur J Clin Nutr. 2001;55:651–6.
17. Chen TT, Li L, Chung DH, Allen CD, Torti SV, Torti FM, Cyster JG, Chen CY, Brodsky FM, et al. TIM-2 is expressed on B cells and in liver and kidney and is a receptor for H-ferritin endocytosis. J Exp Med. 2005;202:955–65.
18. Ramm GA, Britton RS, O'Neill R, Bacon BR. Identification and characterization of a receptor for tissue ferritin on activated rat lipocytes. J Clin Invest. 1994;94:9–15.
19. Hulet SW, Powers S, Connor JR. Distribution of transferrin and ferritin binding in normal and multiple sclerotic human brains. J Neurol Sci. 1999;165:48–55.
20. Ragland M, Briat JF, Gagnon J, Laulhere JP, Massenet O, Theil EC. Evidence for conservation of ferritin sequences among plants and animals and for a transit peptide in soybean. J Biol Chem. 1990;265:18339–44.

21. Smith PKKR, Hermanson GT, Mallia AK, Gartner FH, Provenzano MD, Fujimoto EK, Goeke NM, Olson BJ, Klenk DC. Measurement of protein using bicinchoninic acid. Anal Biochem. 1985;150:76–85.
22. Goldstein JL, Brown MS. Binding and degradation of low density lipoproteins by cultured human fibroblasts. Comparison of cells from a normal subject and from a patient with homozygous familial hypercholesterolemia. J Biol Chem. 1974;249:5153–62.
23. Bos CR, Shank SL, Snider MD. Role of clathrin-coated vesicles in glycoprotein transport from the cell surface to the Golgi complex. J Biol Chem. 1995;270:665–71.
24. Zhao B, Li Y, Buono C, Waldo SW, Jones NL, Mori M, Kruth HS. Constitutive receptor-independent low density lipoprotein uptake and cholesterol accumulation by macrophages differentiated from human monocytes with macrophage-colony-stimulating factor (M-CSF). J Biol Chem. 2006;281:15757–62.
25. Dugast M, Toussaint H, Dousset C, Benaroch P. AP2 clathrin adaptor complex, but not AP1, controls the access of the major histocompatibility complex (MHC) class II to endosomes. J Biol Chem. 2005;280:19656–64.
26. Arredondo M, Tapia V, Rojas A, Aguirre P, Reyes F, Marzolo MP, Núñez MT. Apical distribution of HFE-beta2-microglobulin is associated with inhibition of apical iron uptake in intestinal epithelia cells. Biometals. 2006;19:379–88.
27. Aguirre P, Mena N, Tapia V, Arredondo M, Núñez MT. Iron homeostasis in neuronal cells: a role for IREG1. BMC Neurosci. 2005;6:3.
28. Gelvan D, Fibach E, Meyron-Holtz EG, Konijn AM. Ferritin uptake by human erythroid precursors is a regulated iron uptake pathway. Blood. 1996;88:3200–7.
29. Breuer W, Epsztejn S, Cabantchik ZI. Iron acquired from transferrin by K562 cells is delivered into a cytoplasmic pool of chelatable iron(II). J Biol Chem. 1995;270:24209–15.
30. Epsztejn S, Kakhlon O, Glickstein H, Breuer W, Cabantchik I. Fluorescence analysis of the labile iron pool of mammalian cells. Anal Biochem. 1997;248:31–40.
31. Kakhlon O, Cabantchik ZI. The labile iron pool: characterization, measurement, and participation in cellular processes(1). Free Radic Biol Med. 2002;33:1037–46.
32. Arredondo M, Muñoz P, Mura CV, Núñez MT. DMT1, a physiologically relevant apical Cu1+ transporter of intestinal cells. Am J Physiol Cell Physiol. 2003;284:C1525–30.
33. Daukas G, Zigmond SH. Inhibition of receptor-mediated but not fluid-phase endocytosis in polymorphonuclear leukocytes. J Cell Biol. 1985;101:1673–9.
34. Hansen S, Sandvig K, van Deurs B. Clathrin and HA2 adaptors: effects of potassium depletion, hypertonic medium, and cytosol acidification. J Cell Biol. 1993;121:61–72.
35. Sandvig K, Olsnes S, Petersen OW, van Deurs B. Acidification of the cytosol inhibits endocytosis from coated pits. J Cell Biol. 1987;105:679–89.
36. Rothberg KG, Ying YS, Kamen BA, Anderson RG. Cholesterol controls the clustering of the glycophospholipid-anchored membrane receptor for 5-methyltetrahydrofolate. J Cell Biol. 1990;111:2931–8.
37. Rothberg KG, Heuser JE, Donzell WC, Ying YS, Glenney JR, Anderson RG. Caveolin, a protein component of caveolae membrane coats. Cell. 1992;68:673–82.
38. Orlandi PA, Fishman PH. Filipin-dependent inhibition of cholera toxin: evidence for toxin internalization and activation through caveolae-like domains. J Cell Biol. 1998;141:905–15.
39. Benlounes N, Chedid R, Thuillier F, Desjeux JF, Rousselet F, Heyman M. Intestinal transport and processing of immunoglobulin G in the neonatal and adult rat. Biol Neonate. 1995;67:254–63.
40. Rodewald R, Kraehenbuhl JP. Receptor-mediated transport of IgG. J Cell Biol. 1984;99:s159–64.
41. Ragland M, Theil EC. Ferritin (mRNA, protein) and iron concentrations during soybean nodule development. Plant Mol Biol. 1993;21:555–60.
42. Harrison PM, Arosio P. The ferritins: molecular properties, iron storage function and cellular regulation. Biochim Biophys Acta. 1996;1275:161–203.
43. Liu X, Theil EC. Ferritins: dynamic management of biological iron and oxygen chemistry. Acc Chem Res. 2005;38:167–75.
44. Hancock JF. Plant evolution and the origin of crop species. 2nd ed. Cambridge (MA): CABI Publishing; 2004.
45. Arredondo M, Muñoz P, Mura CV, Núñez MT. HFE inhibits apical iron uptake by intestinal epithelial (Caco-2) cells. FASEB J. 2001;15:1276–8.
46. Mendiburo MJ, Flores S, Pizarro F, Arredondo M. Heme oxygenase 1 overexpression increases iron fluxes in caco-2 cells. Biol Res. 2006;39:195–7.
47. Adams PC, Chau LA. Hepatic ferritin uptake and hepatic iron. Hepatology. 1990;11:805–8.
48. Hunt JR, Roughead ZK. Nonheme-iron absorption, fecal ferritin excretion, and blood indexes of iron status in women consuming controlled lactoovovegetarian diets for 8 wk. Am J Clin Nutr. 1999;69:944–52.